Next Energy 1 (2023) 100001

Contents lists available at ScienceDirect

Next Energy

journal homepage: www.sciencedirect.com/journal/next-energy

Protocol

Accelerated test protocols to predict service life and durability of solid oxide fuel cells

Emir Dogdibegovic[a], Yudong Wang[a,b], Xiao-Dong Zhou[a,b,*]

[a] Department of Chemical Engineering, University of South Carolina, Columbia, SC 29208, USA
[b] Institute for Materials Research and Innovation, University of Louisiana at Lafayette, LA 70504, USA

ARTICLE INFO

Keywords:
Accelerated test protocols
Solid oxide fuel cells
Durability

ABSTRACT

Reliable accelerated test protocols are needed for solid oxide fuel cell research to facilitate rapid learning on key durability issues, identify potential modes of failure expeditiously, and eventually predict the calendar lifetime of an electrochemical cell. In this work, solid oxide fuel cells operated at a constant current density were compared to cells undergoing accelerated measurements, which are composed of intermittent current injection to the cell. A general accelerated test profile was developed by cycling a solid oxide fuel cell from open circuit to a predetermined operating current density that is the same as the current density during a steady-state operation, to accelerate the local redox environment. The following parameters were studied: current density, operation temperature, moist level, sintering temperature, cycling current, cycling frequency, and operation time. Up to 1,320,000 cycles were generated in this work. The cell degradation was accelerated by nearly 10 times, suggesting the feasibility of using this protocol for acceleration test to predict life performance and durability of solid oxide fuel cells.

Introduction

Solid oxide cells (SOCs) have attracted increasing attention in realizing the "Power-to-X" concept [1], where X can refer to H_2, NH_3, synthetic fuels, or other chemicals, primarily because of their (1) cost-effectiveness, (2) ability to use waste heat to reduce electricity input, and (3) feasibility for co-electrolysis of CO_2 and H_2O to produce syngas at a large scale [2]. An SOC can operate in an electrolysis mode as a solid oxide electrolysis cell (SOEC) with ~ 100 % selectivity; and it can be reversibly switched between the SOEC mode to produce X and the solid oxide fuel cell (SOFC) mode to generate electricity [3]. During the past two decades, numerous processes have been made to scale up this technology for power generation, hydrogen production, and carbon management. The current research and development (R&D) in SOCs focuses on the pursuit of further promoting highly durable, robust, reliable, and active SOC materials and systems.

A long-lasting challenge in SOC R&D is to develop accelerated test protocols because an operation of SOCs under its normal conditions for tens of thousands of hours could be impractical and costly. As a result, reliable accelerated test protocols (ATPs) are needed to facilitate rapid learning on key durability and reliability issues to predict the calendar lifetime of an SOC. Care, however, must be taken to develop ATPs to ensure that (1) there are no new failure mechanisms introduced, which would be unrealistic in a real SOC environment and (2) detailed and reliable examinations are performed on single cells or stacks under the steady-state operation to provide reproducible baselines. Performance degradation in an SOC may attribute to the evolution of electrode materials. At the fuel electrode side, the operation temperatures, applied loading, and steam concentrations are the key factors influencing Ni-coarsening [4]. On the other hand, strontium segregation is considered as a dominating mechanism of the performance degradation in Sr-containing oxygen-electrode without a poisoning atmosphere. Extensive research has been carried out to understand the role of Sr segregation on cell performance and approaches to suppress Sr-segregation [5], but few publications report how to accelerate such segregation and subsequently develop the ATPs.

In this work, cells operated at a constant current density were compared to cells undergoing newly developed ATPs, which are composed of intermittent current injection to the cell. **A general accelerated test profile** was developed by cycling an SOFC from open circuit (current = 0) to a predetermined operating current density that is the same as the current density during a steady-state operation. The motivation of this concept was originated from our prior work [6,7] which reported that (La,Sr)MnO_3, an oxygen electrode for SOCs, underwent enhanced densification rates upon the exposure of repeated oxygen partial pressure cycles. Cycling pO_2 creates transient cation and oxygen vacancies well above the equilibrium concentration, resulting in

* Corresponding author at: Department of Chemical Engineering, University of South Carolina, Columbia, SC 29208, USA.
E-mail address: zhou@louisiana.edu (X.-D. Zhou).

https://doi.org/10.1016/j.nxener.2022.100001
Received 27 November 2022; Received in revised form 6 December 2022; Accepted 6 December 2022

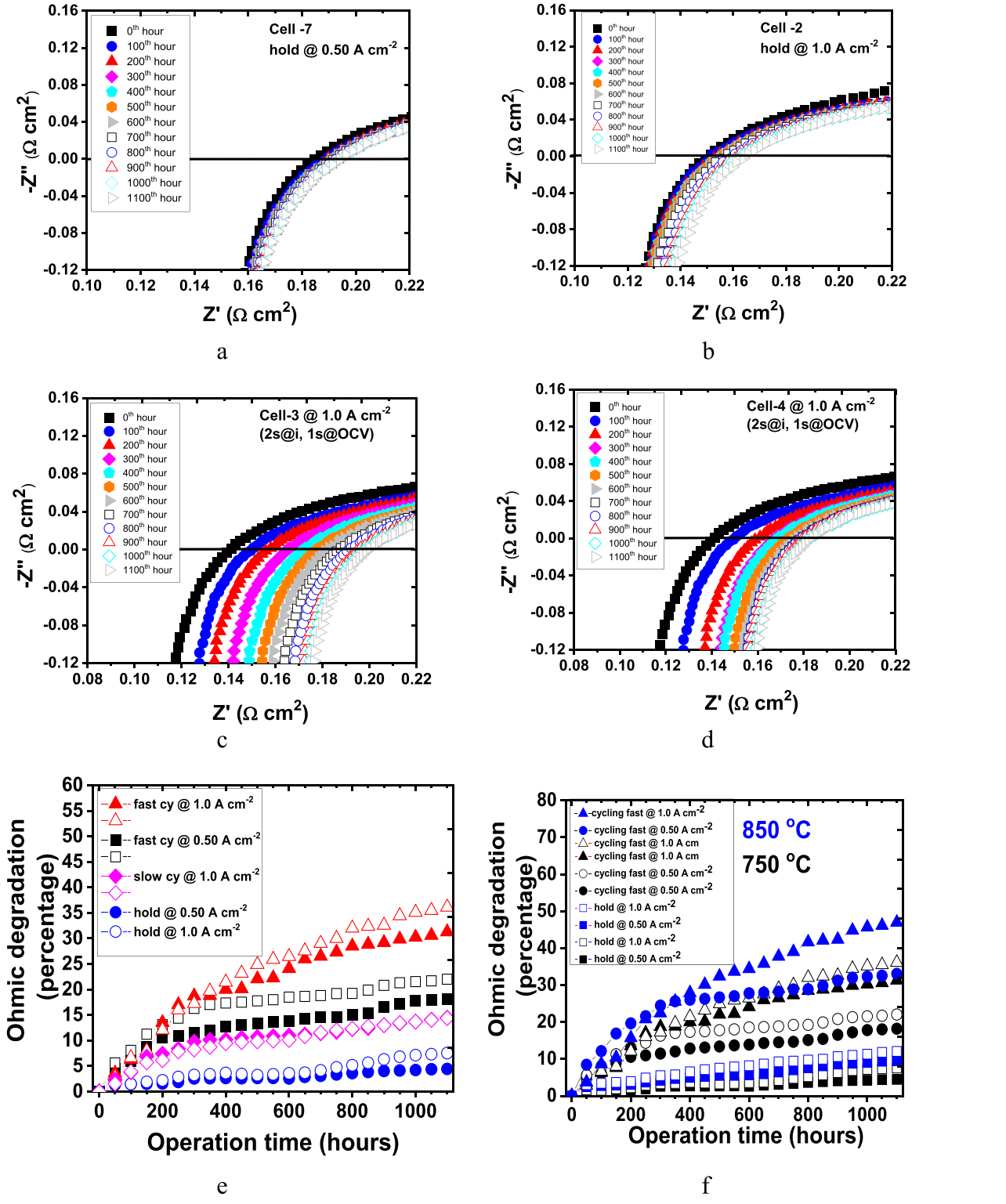

Fig. 1. The evolution of EIS spectra of LSCF-based cells under a constant current operation, 0.5 A/cm^2 (a) and 1 A/cm^2 (b). The evolution of EIS spectra of two cells which were operated at 1 A/cm^2 for 2 s, then held at OCV for 1 s, up to 1100 h. (c) and (d). (e) A summary plot of the percentage increase of ohmic ASR as a function of time for the cells cycling at various conditions. Results shown in (a)–(e) were acquired at 750 °C. (f) A comparison of operation temperature on the cycling effects between 750 and 850 °C. *Note that two cells were measured at the same condition to evaluate cycling effect as an accelerated test as shown in Fig. 1 e and f.*

enhanced mobility [6]. The cycle frequency is an important parameter for accelerated tests. Two frequencies adopted: fast cycle was done by holding a cell at an operating current for 2 s and then at the open circuit for 1 s, while the slow cycle was holding for 20 s at an operating current and 5 s at open circuit condition. For 300 h of operation, the fast cycle is equivalent to 360,000 cycles; while for 1,100 h of operation, 1,320,000 cycles were generated. It is worth noting again that the current density for cells undergoing ATPs was the same in cells operated at constant current density. Two cells were measured for each condition to study reproducibility and consistency in the SOFC mode.

Results and Discussion

Initial research focused on acquiring the baseline results by applying a constant current on cells with $La_{0.6}Sr_{0.4}Co_{0.2}Fe_{0.8}O_3$ (LSCF) cathode. Two current densities were used, 0.5 and 1.0 A/cm^2. Fig. 1**a** and **b** show the electrochemical impedance spectra (EIS) of the cells under a steady-state operation. The ohmic area specific resistance (ASR) of cells is the high-frequency interception of the EIS spectrum with the Z′-axis (x-axis). The higher current density (1.0 A/cm^2) leads to a slight increase in the ohmic ASR, suggesting the degradation rate of cell performance increases with increasing operation current under a steady-state operation. Fig. 1**c** and **d** show the evolution of ohmic ASR vs. time under cycling. Two cells (Fig. 1**c** and **d**) were used with the same experimental conditions. Fig. 1**e** shows a summary of the percentage increase of the ohmic ASR as a function of time for the cells cycling at various conditions. Results shown in Fig. 1 **(a)–(e)** were obtained at 750 °C. Fig. 1(**f**) is a comparison of effects of operation temperature (750 vs. 850 °C) on the performance degradation.

The increase in ohmic ASR is indeed accelerated during cycling even though the operating temperature and current density remained the same in the steady-state operation, suggesting the effectiveness of accelerating test in cycling measurements. Results shown in Fig. 1 and Table 1 suggest that the acceleration effect is more dominant with a higher cycling current, faster cycling frequency, or a higher operation temperature (e.g., 850 °C):

1. **Cycling frequency**. A fast cycle by holding a cell at an operating current for 2 s and then at the open circuit for 1 s results in more effective acceleration than the slow cycle (Fig. 1e and Table 1).
2. **Current density**. In addition to the cycling frequency, the current density plays an equally important role on the acceleration. When the cells were under fast cycle, the current density of 1 A/cm^2 led to ~ 35 % increase in ohmic ASR of two cells, in comparison with ~ 17 % increase for the cells operating at 0.5 A/cm^2 (Fig. 1e and Table 1).
3. **Operating temperature**. The acceleration effect is more profound at a higher operating temperature, e.g. 850 °C, than 750 °C (Fig. 1f).

The Gd-doped ceria (GDC) layer was used to block interaction between LSCF and the yttrium-stabilized zirconia (YSZ) electrolyte [8]. The interaction between LSCF and YSZ may lead to the formation of insulating $SrZrO_3$ or the diffusion of Zr into LSCF [9]. Mechanism to understand Sr-migration through GDC to reach the interface between YSZ and GDC requires additional investigating. The Sr concentration, shown in Fig. 2**b** at the interfaces is much higher in the cells under a faster cycling measurement. Moreover, a higher current density results in a faster segregation, thus a greater increase in the ohmic loss. The Sr-segregation was not detected at the YSZ/GDC interfaces in the cell before operation. When analyzing the presence of Sr, it is necessary to couple it with La/Co/Fe since the electron beam during EDS analysis may reach to the cathode. If both La and Sr are detected with a ratio close to 6/4, it suggests that this assumption is true, especially if Co and Fe are detected in a corresponding ratio, following the formula of the cathode. None of La/Co/Fe was observed at the YSZ/GDC interfaces. Multiple cells are needed to study the reliability and reproducibility of each cycling condition, as listed in Table 1. The Sr segregation at the YSZ/GDC interfaces is closely correlated with the decrease in cell performance that is summarized in Table 1.

The fast-cycling test achieves same ohmic degradation under 1,000-h steady-state operation within 100 h by accelerating Sr segregation and migration. This means that the accelerated test protocols are applicable to reduce the testing time by almost 10 times without changing the degradation mechanisms. It appears that the measurements between 200 and 1,000-h periods can be used to simulate the steady-state operation up to 2,000 and 10,000 h.

Further research was carried to investigate the role of cathode sintering temperature and operating temperature on the applicability of accelerated test. Fig. 2(c) shows the role of the sintering temperature on the cell performance upon cycling with LSCF being sintered at 900 or 1,080 °C. Higher sintering temperature resulted in an improved performance and performance stability. Fig. 2(d) shows the cycling effect at a higher operation temperature (850 °C), which leads to a more rapid degradation than that at 750 °C. A raised operating temperature from 750 °C to 850 °C can accelerate the electrode degradation. Fig. 2(e) and (f) are DRT analysis showing how the polarization resistance corresponding to different relaxation frequency changes. The dominating peaks, P1c–P3c, are generated by the different cathode processes and the area under individual peak is proportional to the polarization resistance that the corresponding process contributes [10–12]. The peaks

Table 1
Percentage of the increase in ohmic ASR and cell power density (PD) as a function of operating time, cycling current, cycling frequency, and H_2O% in air for LSCF-cells at 750 °C.

Operating conditions	Ohmic ASR and power density (PD) changes (%)		H_2O% in air	250 h	600 h	1100 h
Hold @ 0.50 A cm^{-2}	Baseline, low current (J)	Ohmic	0.6	1.9	2.6	4.5
		PD		1.3	2.3	3.6
Hold @ 1.0 A cm^{-2}	Baseline, high current (J)	Ohmic	0.6	2.9	3.5	7.5
		PD		1.8	4.0	6.5
Cycling @ 0.50 A cm^{-2}; 2 s@loading, 1 s@OCV	Fast cycle; low *J*	Ohmic	0.6	11.0	13.7	18.2
		PD		4.2	8.4	13.3
Cycling @0.50 A cm^{-2}; 2 s@loading, 1 s@OCV	Fast cycle; low *J*	Ohmic	0.6	14.4	18.5	22.0
		PD		4.2	8.3	13.2
Cycling @ 1.0 A cm^{-2}; 2 s@loading, 1 s@OCV	Fast cycle; high *J*	Ohmic	0.6	17.0	24.1	31.2
		PD		5.6	11	17.4
Cycling @ 1.0 A cm^{-2}; 2 s@loading, 1 s@OCV	Fast cycle; high *J*	Ohmic	0.6	16.0	26.5	36.0
		PD		5.6	11	17.5
Cycling @1.0 A cm^{-2}; 20 s@loading, 5 s@OCV	Slow cycle; high *J*	Ohmic	0.6	8.4	10.1	14.0
		PD		2	4.5	7.8
Cycling @1.0 A cm^{-2}; 20 s@loading, 5 s@OCV	Slow cycle; high *J*	Ohmic	0.6	7.9	10.3	14.4
		PD		2.3	5.0	8.2
Cycling @ 1.0 A cm^{-2}; 2 s@loading, 1 s@OCV	Fast cycle; high *J*, wet air	Ohmic	3.0	20.1	31.5	39.5
		PD		9.2	18.9	23.1
Hold @ 1.0 A cm^{-2}	Constant & high *J*, wet air	Ohmic	3.0	5.3	7.1	9.2
		PD		1.8	3.6	5.2
Cycling @1.0 A cm^{-2}; 2 s@loading, 1 s@OCV	Fast cycle; high *J*, dry air	Ohmic	0	9.4	18.4	21.6
		PD		4.4	7.6	9.9
Hold @ 1.0 A cm^{-2}	Constant & high *J*, dry air	Ohmic	0	1.1	2.9	3.9
		PD		1.1	1.4	1.4

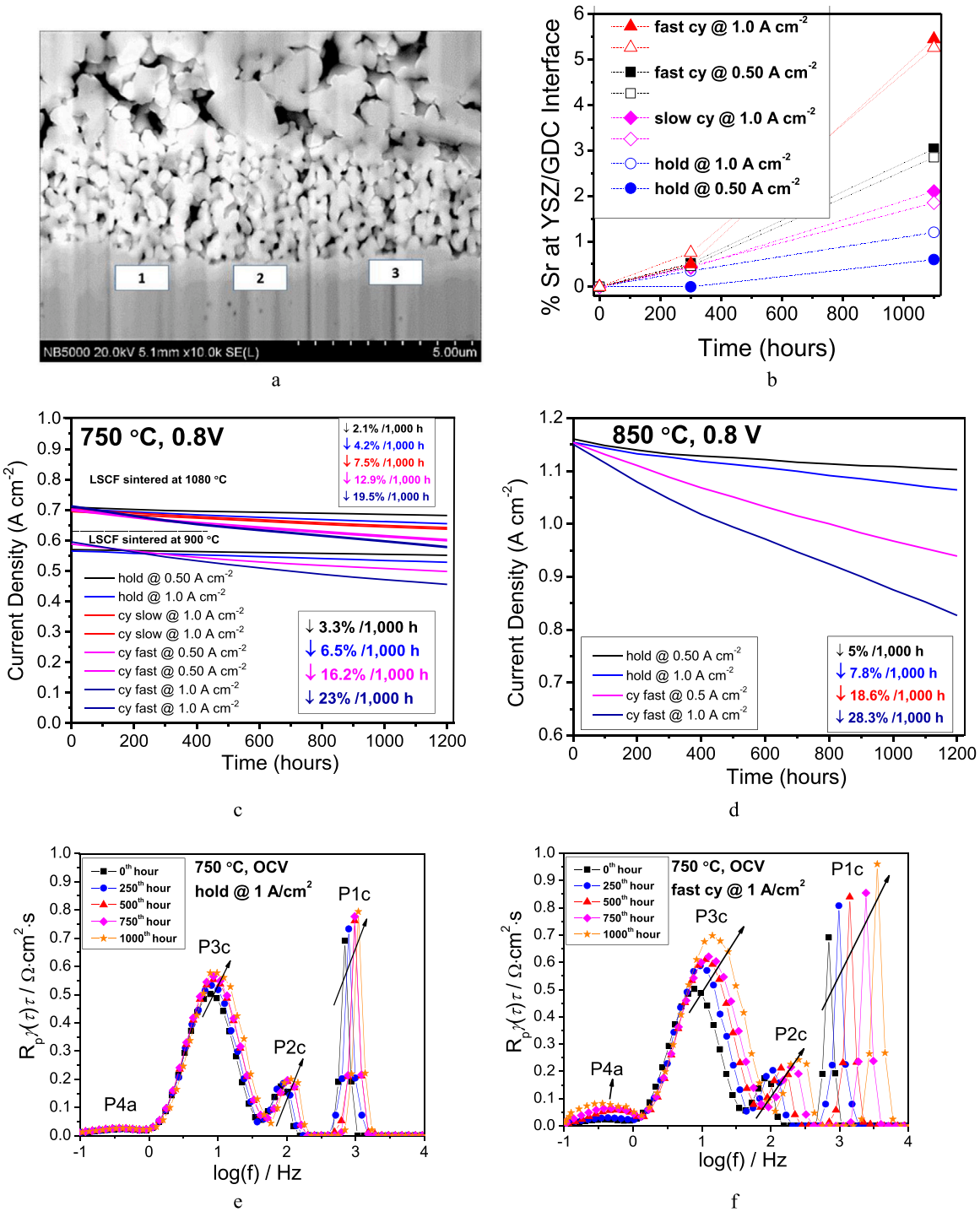

Fig. 2. (a) A cross-sectional image of LSCF-based cells for the analysis of GDC/YSZ interfaces (b) Sr concentration at the interfaces as a function of time under various operation conditions. (c) Cell performance upon cycling with LSCF sintered at 900 or 1080 °C. (d) Cycling effect at a higher operation temperature (850 °C). (e) and (f) are DRT analysis showing the evolution of ASR_{ohm} and ASR_p vs. time at 750 °C. *Note the anode peaks (P4a) slightly change upon cycling, while it remains constant and a low value at a constant current.*

shift to the high frequency under both cases, while the area increases significantly under cycling condition. The cycling operation accelerates the cathode degradation because P4a, which is assigned to anodic processes, is negligible in this case [12]. P4a does evolve with time during the cycling measurements, which can be potentially used to develop accelerated test protocols for anode.

The Sr in LSCF is known to segregate from the bulk phase and migrate to the GDC/YSZ interface, which causes an increase in both ohmic and electrode resistances, thus cell performance degradation. Electrode polarization is shown in Fig. 3**a**. As shown in Fig. 3**a**, the electrode polarization resistance (R_p) value remains stable under a steady-state operation, however it increases up to 5.5 % under slow cycling and 19.7 % under fast cycling at 1 A/cm^2 for 1,000 h. The change of polarization resistance is less than that of ohmic ASR, suggesting the electrode is still active during long term operation.

The Sr segregation and migration is impacted by the humidity in air, which was then examined in our research. Indeed, as shown in Fig. 3**b**, for cell under a steady-state operation, increasing the humidity in air

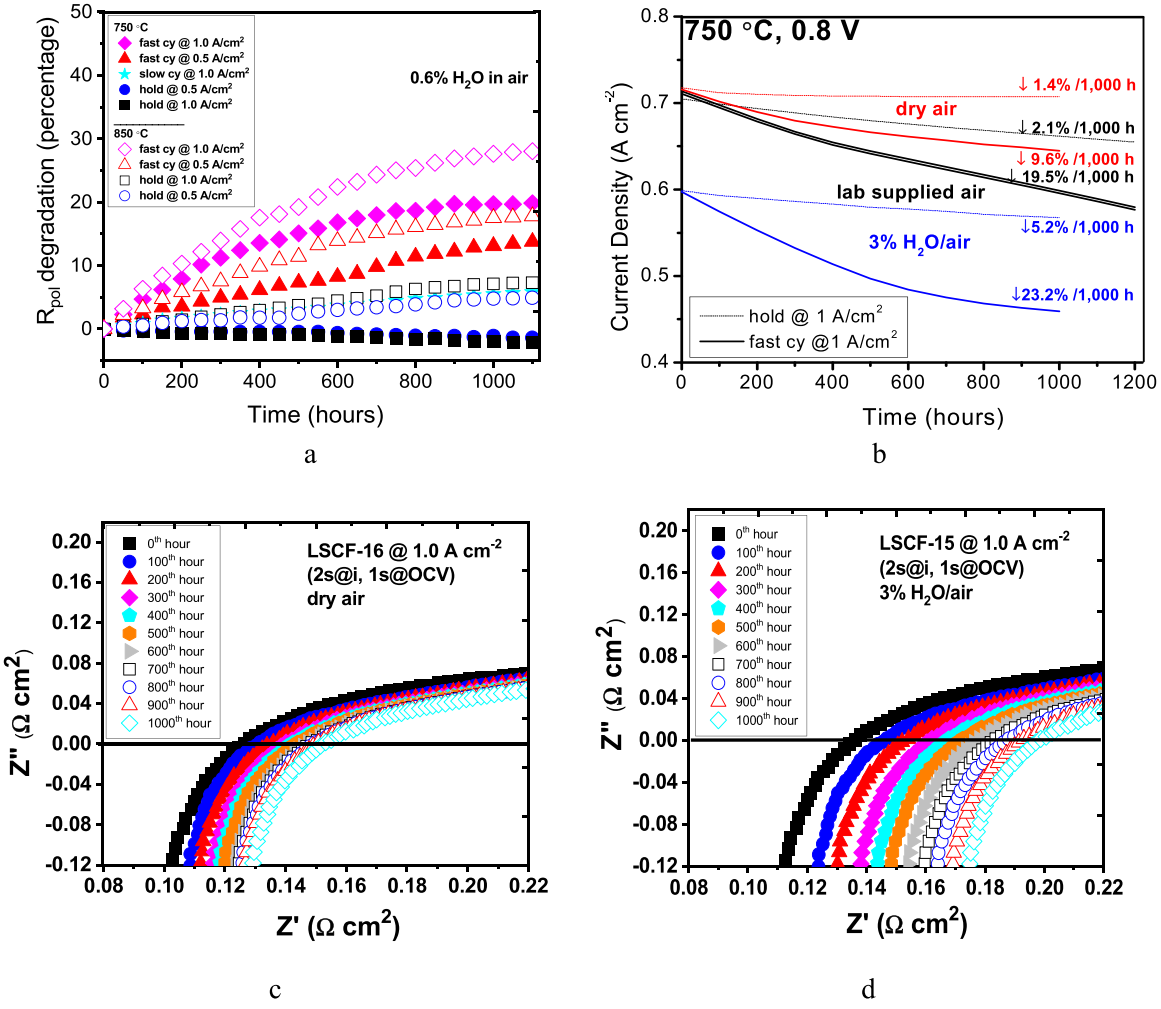

Fig. 3. (a) Electrode polarization resistance, (b) cell I-V plots, and EIS (c) and (d) as a function of time during cycling measurements with various moisture content (fast cycle and high current density).

stream did decrease the cell performance when the cell was holding at 1 A/cm^2. Fig. 3(b) shows cells were operated at a constant 1 A/cm^2 in dry air, 0.6 % H_2O/Air, and 3 % air/water, which exhibited 1.4 %, 2.1 %, and 5.2 % performance degradation per 1,000 h, respectively. In comparison, the fast cycling at 1 A/cm^2, the degradation rate increased to 9.6 %, 19.5 %, and 23.2 % per 1,000 h, respectively. Regardless of the humidity in electrode, the cycling test results in ~ 4–9 times performance degradation of the constant current operation.

Understanding the mechanism for the cycling effects on the oxygen electrode properties, and thus cell performance, is being undertaken. In steady-state, kinetic demixing is known to occur, which was first reported by Schmalzried et al. in 1979 on a model oxide system, $(Co_{1-x}Mg_x)O$, where Co is the faster moving component than Mg [13]. Moreover, chemical transformation [14–16], and cation kinetic demixing due to external force were observed in the presence of electric field [17], chemical potential gradients [18,19], and stress-driven segregation [20]. It is known that the electric field created by the excess charges and oxygen vacancies at the electrode surface is a driving force for Sr segregation [21,22]. By applying a steady cathodic current, the electrode is under more reducing condition [15], leading to an increasing amount of oxygen vacancies at the electrode surface and thus faster surface segregation comparing to the equilibrium state [23,24]. The Sr flux from the bulk to the surface is coupled with the charge transport in the electrode [25], shown as the term, $-s_{Sr,h}\nabla\tilde{\mu}_{h^o}$, in $J_{Sr} = -s_{Sr,Sr}\nabla\tilde{\mu}_{Sr^{2+}} - s_{Sr,h}\nabla\tilde{\mu}_{h^o}$, where $\tilde{\mu}_{Sr^{2+}}$ is the electrochemical potential of Sr^{2+} and $\tilde{\mu}_{h^o}$ is the electrochemical potential of electron hole. The coupling coefficient $s_{Sr,h}$ is proportional to the electron hole concentration [25], which is higher at OCV than under an SOFC operation. On the other hand, $\nabla\tilde{\mu}_{h^o}$ is nearly 0 under OCV and this gradient can reach a high value under transition state. Therefore, an effective approach for a high Sr flux and accelerated Sr transport is to keep the electrode under transition state. The relaxation of charge transport in the electrode is dominated by the sluggish redistribution of oxygen ions. The period to remain the electrode under non-steady state can be estimated by the time for oxygen ion diffusion (~ 10^0 s magnitude). The cycling operation with a period of 3 s keeps the cell under non-steady state all the time (Fig. S4); it shows faster Sr segregation and performance degradation than the slow cycling with a period of 25 s. Therefore, the fast cycling (2 s@loading, 1 s@OCV) achieves faster Sr migration than slow cycling and it offers a proper and significant protocol for accelerated SOFC tests.

Conclusion

In summary, for an LSCF-based oxygen electrode, the following parameters were studied: current density, operation temperature, moist level, sintering temperature, cycling current, cycling frequency, and operation time. During the steady-state operation, a higher operation current (1 A/cm^2) results in a slightly higher ohmic ASR than the cell operated at 0.5 A/cm^2. An accelerated increase in ohmic ASR was observed during the use of ATPs. The acceleration effect is more dominant with a higher cycling current, faster cycling frequency, a higher

operation temperature (e.g., 850 °C), and a greater moisture level. When the cells were tested under ATPs at the fast cycle at 850 °C with the presence of 3 % H_2O in the air stream, it was observed that the cell degradation was accelerated by nearly 10 ×, suggesting the feasibility of using this protocol for acceleration test. The mechanism for the acceleration is linked with accelerated Sr segregation from LSCF and deposition at the YSZ/doped ceria interfaces, which was also observed in cells operated under stead-state conditions.

Experimental

The bilayers tapes of NiO-YSZ anode layers and YSZ ($Y_{0.08}Zr_{0.92}O_{1.96}$) electrolyte layer were prepared via tape-casting and lamination process. The bilayer was cut into button cells with 25 mm in diameter after sintering. The anode support has a thickness of ~ 400 µm and the dense electrolyte has a thickness of about 8 µm. The GDC ($Gd_{0.2}Ce_{0.8}O_{1.9}$) interlayer was screen-printed on top of the electrolyte and sintered at 1,200 °C for 2 h. LSCF ($La_{0.6}Sr_{0.4}Co_{0.2}Fe_{0.8}O_3$) was screen-printed and sintered at 1,080 °C as cathode. The active area of LSCF electrode is 2 cm^2. A gold grid was coated on the LSCF as the cathode current collector. Nickel mesh is attached to the anode support as the anode current collector. The current collectors are sintered at 900 °C for 30 min.

The anode supported cell was electrically connected to four Pt lead wires to perform electrochemical measurement. The cell was set on an alumina tube and the edge of the cell was sealed with glass. The glass was sintered at 850 °C for 1 h and the furnace cooled down to the operating temperature for electrochemical operation. The anode chamber is fed with 200 sccm fuel flow humidified by a water bubbler at room temperature to achieve 3 % water vapor pressure. The flowrate of air is controlled at 500 sccm from the compressor. The wet air is obtained by passing the house air through the water bubbler at room temperature, while the dry air is supplied from the cylinder. The electrochemical measurements were carried out by a Biologic VMP3 multi-channel potentiostat (Bio-Logic USA, Knoxville, TN) equipped with external current boosters. The electrochemical impedance spectroscopy (EIS) is performed by applying an alternative current of 10 mA/cm^2 and a frequency from 0.1 Hz to 50 kHz. Distribution of relaxation time analysis is performed with FTIKREG program and a regulation number of 1×10^{-2} [11,26]. The accelerated test is performed by cycling between a constant output current and open circuit voltage in a short period. IV and impedance of cell is collected every 50 h for long term constant current or cycling test of up to 1,100 h. The cell components and interfaces are studied was performed on a nano-DUE'T double-beam NB5000 microscope (Hitachi) equipped with focused ion beam and EDS analysis.

Declaration of Competing Interest

The authors declare that they have no known competing financial interests or personal relationships that could have appeared to influence the work reported in this paper.

Acknowledgement

We greatly appreciate the support of this work by the U.S. Department of Energy's Office of Fossil Energy and Carbon Management under DE-FE0026097 and DE-FE0032110. Part of this work is supported by U.S. National Science Foundation under NSF-2119688.

Appendix A. Supporting information

Supplementary data associated with this article can be found in the online version at doi:10.1016/j.nxener.2022.100001.

References

[1] A. Hauch, R. Küngas, P. Blennow, A.B. Hansen, J.B. Hansen, B.V. Mathiesen, M.B. Mogensen, Recent advances in solid oxide cell technology for electrolysis, Science 370 (6513) (2020).
[2] X.-D. Zhou, Kill two problems with one dual-ion cell, Joule 3 (11) (2019) 2595–2597.
[3] R. Küngas, Review—electrochemical CO_2 reduction for CO production: comparison of low- and high-temperature electrolysis technologies, J. Electrochem. Soc. 167 (4) (2020) 044508.
[4] A. Ploner, A. Hagen, A. Hauch, Study of operating parameters for accelerated anode degradation in SOFCs, Fuel Cells 17 (4) (2017) 498–507.
[5] H. Wang, K.J. Yakal-Kremski, T. Yeh, G.M. Rupp, A. Limbeck, J. Fleig, S.A. Barnett, Mechanisms of performance degradation of (La,Sr)(Co,Fe)$O_{3-\delta}$ solid oxide fuel cell cathodes, J. Electrochem. Soc. 163 (6) (2016) F581.
[6] B.P. McCarthy, L.R. Pederson, H.U. Anderson, X.D. Zhou, P. Singh, G.W. Coffey, E.C. Thomsen, Enhanced shrinkage of lanthanum strontium manganite ($La_{0.90}Sr_{0.10}MnO_{3+d}$) resulting from thermal and oxygen partial pressure cycling, J. Am. Ceram. Soc. 90 (10) (2007) 3255–3262.
[7] B.P. McCarthy, L.R. Pederson, R.E. Williford, X.D. Zhou, Low-temperature densification of lanthanum strontium manganite ($La_{1-x}Sr_xMnO_{3+d}$), x = 0.0–0.20, J. Am. Ceram. Soc. 92 (8) (2009) 1672–1678.
[8] A. Mai, V.A. Haanappel, F. Tietz, D. Stöver, Ferrite-based perovskites as cathode materials for anode-supported solid oxide fuel cells: Part II. Influence of the CGO interlayer, Solid State Ion. 177 (19–25) (2006) 2103–2107.
[9] V. Wilde, H. Störmer, J. Szász, F. Wankmüller, E. Ivers-Tiffée, D. Gerthsen, $Gd_{0.2}Ce_{0.8}O_2$ diffusion barrier layer between ($La_{0.58}Sr_{0.4}$)($Co_{0.2}Fe_{0.8}$)$O_{3-\delta}$ cathode and $Y_{0.16}Zr_{0.84}O_2$ electrolyte for solid oxide fuel cells: effect of barrier layer sintering temperature on microstructure, ACS Appl. Energy Mater. 1 (12) (2018) 6790–6800.
[10] Y. Wang, B. Marchetti, X.-D. Zhou, Call attention to using DRT and EIS to quantify the contributions of solid oxide cell components to the total impedance, Int. J. Hydrog. Energy 47 (83) (2022) 35437–35448.
[11] H. Schichlein, A.C. Müller, M. Voigts, A. Krügel, E. Ivers-Tiffée, Deconvolution of electrochemical impedance spectra for the identification of electrode reaction mechanisms in solid oxide fuel cells, J. Appl. Electrochem. 32 (8) (2002) 875–882.
[12] C. Graves, S.D. Ebbesen, M. Mogensen, Co-electrolysis of CO_2 and H_2O in solid oxide cells: Performance and durability, Solid State Ion. 192 (1) (2011) 398–403.
[13] H. Schmalzried, W. Laqua, P.L. Lin, Crystalline oxide solid-solutions in oxygen potential gradients, Z. Naturfors. Sect. A-J. Phys. Sci. 34 (2) (1979) 192–199.
[14] E. Dogdibegovic, N.S. Alabri, C.J. Wright, J.S. Hardy, C.A. Coyle, S.A. Horlick, W.B. Guan, J.W. Stevenson, X.D. Zhou, Activity and stability of $(Pr_{1-x}Nd_x)_2NiO_4$ as cathodes for solid oxide fuel cells: Part V. In situ studies of phase evolution, J. Electrochem. Soc. 164 (12) (2017) F1115–F1121.
[15] E. Dogdibegovic, Y. Wang, X.-D. Zhou, Origin for electrochemically driven phase transformation in the oxygen electrode for a solid oxide cell, Proc. Natl. Acad. Sci. 119 (45) (2022) e2203256119.
[16] E. Dogdibegovic, C.J. Wright, Y.D. Wang, Q.S. Cai, Y.X. Zhang, G. Tian, S. Yang, J.B. Yang, B. Marchetti, X.D. Zhou, Toward understanding structural stability in Cu-substituted $(Pr_{1-x}Nd_x)_2NiO_{4+d}$ by in situ and operando studies, J. Phys. Chem. C 126 (34) (2022) 14704–14713.
[17] O. Teller, M. Martin, Kinetic demixing of (Co,Ni)O in an electric field, Solid State Ion. 101 (1997) 475–478.
[18] B.P. McCarthy, L.R. Pederson, Y. Chou, X.D. Zhou, W.A. Surdoval, L.C. Wilson, Low-temperature sintering of lanthanum strontium manganite-based contact pastes for SOFCs, J. Power Sources 180 (1) (2008) 294–300.
[19] G. Petot-Ervas, C. Petot, Oxide solid electrolytes under non-equilibrium conditions – interfaces and ageing, Ionics 11 (2005) 189–197.
[20] C. Reinke, W.C. Johnson, Influence of coherency stress on kinetic demixing, J. Am. Ceram. Soc. 78 (10) (1995) 2593–2602.
[21] W. Lee, J.W. Han, Y. Chen, Z. Cai, B. Yildiz, Cation size mismatch and charge interactions drive dopant segregation at the surfaces of manganite perovskites, J. Am. Chem. Soc. 135 (21) (2013) 7909–7925.
[22] H. Ding, A.V. Virkar, M. Liu, F. Liu, Suppression of Sr surface segregation in $La_{1-x}Sr_xCo_{1-y}Fe_yO_{3-\delta}$: a first principles study, Phys. Chem. Chem. Phys. 15 (2) (2013) 489–496.
[23] M.Y. Lu, J.G. Railsback, H. Wang, Q. Liu, Y.A. Chart, S.-L. Zhang, S.A. Barnett, Stable high current density operation of $La_{0.6}Sr_{0.4}Co_{0.2}Fe_{0.8}O_{3-\delta}$ oxygen electrodes, J. Mater. Chem. A 7 (22) (2019) 13531–13539.
[24] T.T. Fister, D.D. Fong, J.A. Eastman, P.M. Baldo, M.J. Highland, P.H. Fuoss, K.R. Balasubramaniam, J.C. Meador, P.A. Salvador, In situ characterization of strontium surface segregation in epitaxial La0.7Sr0.3MnO3 thin films as a function of oxygen partial pressure, Appl. Phys. Lett. 93 (15) (2008) 151904.
[25] M.H.R. Lankhorst, H.J.M. Bouwmeester, H. Verweij, Thermodynamics and transport of ionic and electronic defects in crystalline oxides, J. Am. Ceram. Soc. 80 (9) (1997) 2175–2198.
[26] J. Weese, A reliable and fast method for the solution of Fredhol integral equations of the first kind based on Tikhonov regularization, Comput. Phys. Commun. 69 (1) (1992) 99–111.